**Supplemental Information**

**Appendix 1: Measuring curvature on cortical surface using a lens clock**

The following provides an overview of the process used to take curvature measurements of cortical surface area using the lens clock. The lens clock is a two-legged spherometer, with a central probe that measures plunge distance (Figure S1). To zero out the lens clock, place the probe on a flat surface like a table, gently depress the device until the legs meet the surface, and press the ZERO button.


Figure S1 Image of lens clock being used on the cortical surface of a quartz fragment, indicating the central probe and legs.

1) To measure an artifact, first orient it along the axis of the longest dimension (white arrow). The artifact used in Fig S2-S4 has cortical (grey, textured) and non-cortical (light brown, smooth) surface (Fig S2). Because we are interested in estimating the size of the unworked nodule, we only take measurements from the cortical surface.


Figure S2 Flake with cortical and non-cortical surface indicated.

2) When measuring a cortical surface (core or flake), the probe is placed gently on the surface and depressed until the legs meet the surface. Lens clock readings (green circles) are first taken perpendicular to the axis of maximum dimension (Fig S 2). Reading sites occur at 1 cm intervals along transects (yellow lines) spaced 1 cm apart, with the lens clock legs set astride the transect (white lines). If the probe or legs cannot be securely set on cortical surface, a measure cannot be taken at that location and the site should be ignored (red Xs). Occasionally, measurement sites will include pits or cavities that result in a negative value, because the probe is not depressed beyond the level of the legs. Sites producing negative values should also be ignored. In this image, 6 sites produce successful recordings.

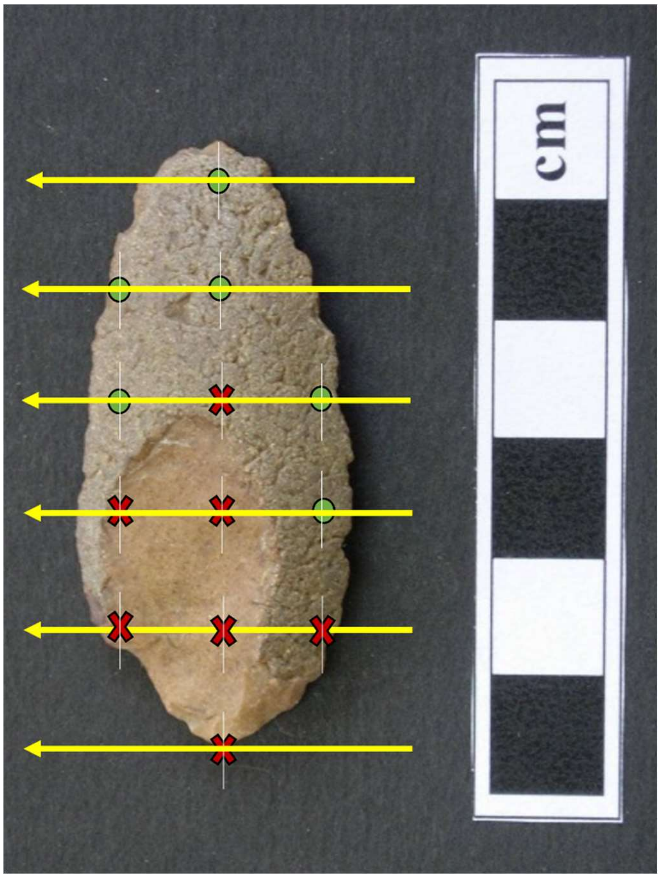


Figure S3 Lens clock measurement sites on cortical flake (perpendicular pass). Sampling transects (yellow arrows), orientation of lens clock legs (white lines), successful measurement sites (green circles) and unsuccessful measurement sites (red circles) are indicated.

3) Once these measurements are completed, take readings (green circles) parallel to the longest axis (Fig S3). Reading sites occur at 1 cm intervals along transects (yellow lines) spaced 1 cm apart, with the lens clock legs set astride the transect (white lines). If the probe or legs cannot be securely set on cortical surface, a measure cannot be taken at that location and the site should be ignored (red Xs). Occasionally, measurement sites will include pits or cavities that result in a negative value, because the probe is not depressed beyond the level of the legs. Sites producing negative values should also be ignored. In this image, 6 sites produce successful recordings.

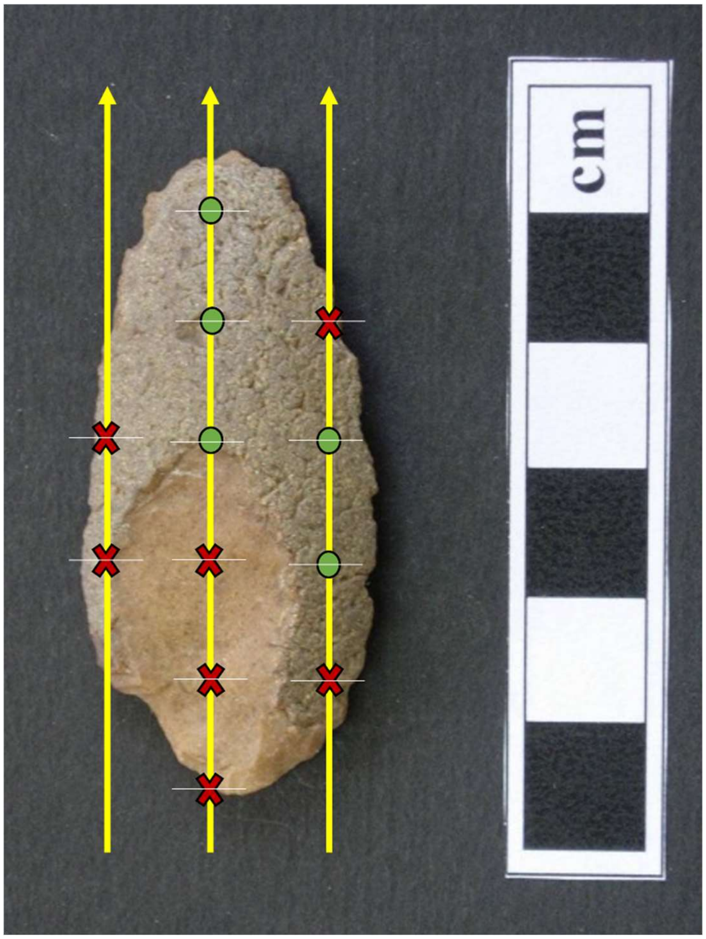


Figure S4 Lens clock measurement sites on cortical flake (parallel pass). Sampling transects (yellow arrows), orientation of lens clock legs (white lines), successful measurement sites (green circles) and unsuccessful measurement sites (red circles) are indicated.

4) Record values in a table, keeping track of the artifact identifier, the Y value (distance between the probe and leg of the lens clock), and S value (the distance of plunge) (Table S1). For this artifact, readings were taken at 11 sites.

Table S1: Example of data recorded from lens clock.

| ART_ID | Y | S |
|---|---|---|
| 21 | 8.785 | 1.71 |
| 21 | 8.785 | 1.49 |
| 21 | 8.785 | 2.56 |
| 21 | 8.785 | 1.48 |
| 21 | 8.785 | 1.24 |
| 21 | 8.785 | 1.88 |
| 21 | 8.785 | 3.62 |
| 21 | 8.785 | 0.72 |
| 21 | 8.785 | 1.74 |
| 21 | 8.785 | 3.31 |
| 21 | 8.785 | 4.28 |

**Appendix 2: Evaluating temporal effects on curvature-based nodule radius estimates**

Given the small number of useable Spring Cave fragments for obtaining curvature measurements, and the similarities of quartz pebble sizes among Elands Bay sources (Bordy et al. 2016), we combined all measured cortical fragments to estimate a single average nodule volume. However, Elands Bay quartz pebbles may not necessarily have been the dominant source of raw materials during both periods. Indeed, if substantial movement were occurring during either period, it may be reasonable to assume that some portion of material might originate elsewhere where raw material characteristics are different.

To evaluate any effects of raw material differences between time periods, we separated the cortical fragments into those from the pre-3000 group (*n*=6), those from the post-1000 BP group (*n*=10), and those from layers not attributable to either group (*n*=2). Using only the fragments that come from the two studied groups (Table S2), estimates for curvature derived nodule radius still align well with the local quartz pebble sizes (Bordy et al. 2016); however, these new estimates lead to a divergence in volume and surface area estimates.

Table S2 Assemblage-specific cortical surface curvature estimates for Spring Cave artifacts and associated geometric measures

| **Assemblage** | **No. of measured fragments** | **No. of curvature measurements** | **Mean curvature-derived nodule radius (mm)** | **Reconstructed nodule volume ($mm^3$)** | **Reconstructed nodule surface area ($mm^2$)** |
|---|---|---|---|---|---|
| <1000 BP | 10 | 330 | 31.2 ± 17 | 91860 | 9845.5 |
| >3000 BP | 6 | 72 | 28.7 ± 15.7 | 50562 | 6612.6 |

When these values are used to calculate the cortex ratio (Table S2), the new values are 0.96 for pre-3000 BP and 0.65 for post-1000 BP. Like the values obtained using the combined curvature estimate, this suggests more movement in the post-1000 period. These show the same statistical properties as well: the cortex ratio from the pre-3000 assemblage still cannot be distinguished from a "complete" assemblage using an experimental dataset (Fig S5), and the difference in cortex ratios between the assemblages (diff=0.3) is statistically significant $p$=0.0069 (Fig S6). In short, the results of the study are robust using fragments from the entire dataset, or restricting them to the assemblages from which they originate. This re-analysis gives us further confidence in the outcome of the study and its wider applicability.

Table S2 Volume, surface area, and cortex ratio estimates for Spring Cave assemblages using assemblage-specific curvature measurements

| **Assemblage** | $n_{quartz}$ | **Total Volume ($mm^3$)** | **Expected Surface Area ($mm^2$)** | **Observed Surface Area ($mm^2$)** | **Cortex Ratio** |
|---|---|---|---|---|---|
| <1000 BP | 273 | 248947.2 | 26677.78 | 17451.9 | 0.65 |
| >3000 BP | 249 | 103698.1 | 13828.1 | 13234.5 | 0.96 |

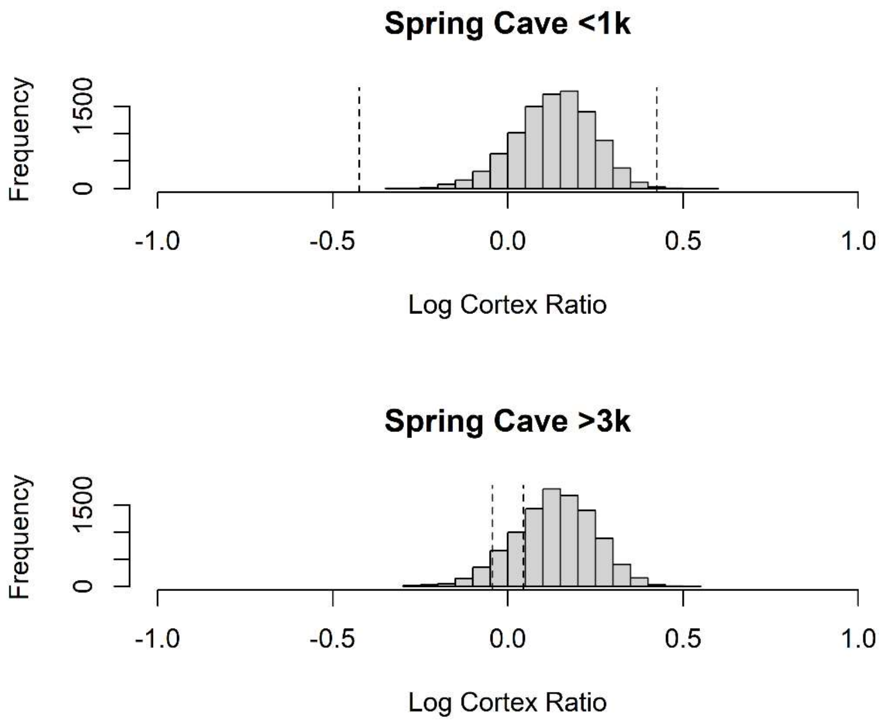


Figure S5 Histograms of log-transformed cortex ratios generated using randomly sampled artifacts from a "complete" experimental assemblage. Dotted line indicates difference between log-transformed observed cortex ratios and 0 for two-tailed probability.

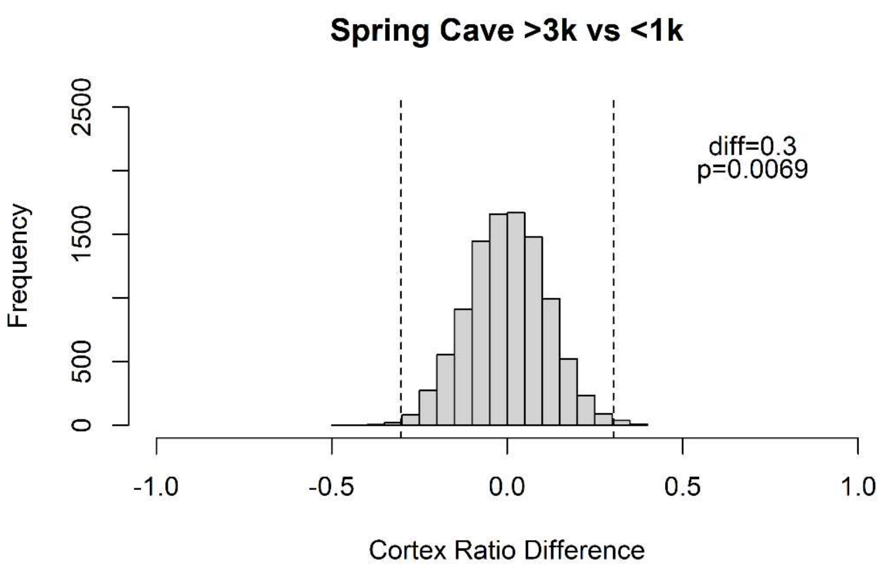


Figure S6 Histogram of differences in cortex ratios between Monte Carlo resampled lithic artifact groups from Spring Cave. Dotted lines indicate observed difference between groups for two-tailed probability (±0.3).